

Quantum sensing and communication – error reduction via interferometry

Cosmo Lupo^{1,2,*} and Zixin Huang^{3,4,†}

¹*Dipartimento Interateneo di Fisica, Politecnico & Università di Bari, 70126, Bari, Italy*

²*INFN, Sezione di Bari, 70126 Bari, Italy*

³*School of Mathematical and Physical Sciences, Macquarie University, NSW 2109, Australia*

⁴*Centre for Quantum Software and Information,*

Faculty of Engineering and IT, University of Technology, Sydney, Australia

(Dated: October 3, 2023)

Dephasing is a main noise mechanism that afflicts quantum information, it reduces visibility, and destroys coherence and entanglement. Here we propose a hardware scheme to mitigate the effects of dephasing in an optical setup. Our scheme uses only passive linear optics and ancillary vacuum modes, and we do not need ancillary photon sources or entanglement. It exploits constructive and destructive interference to partially cancel the detrimental effects of statistically independent noise sources. We apply our approach to preserve coherence in single-photon states, to phase-stabilise stellar interferometry, and to enhance entanglement distribution. For some of these examples, our error mitigation scheme achieves unit fidelity in the asymptotic limit, and such a limit is rapidly approached for only a few ancillary optical modes. For stellar interferometry, our scheme reduces the effect of noise by a quadratic factor.

I. INTRODUCTION

When information is encoded into quantum states, there are tasks in computing [1–5] sensing [6–10], and communication [11–13], that can be accomplished in ways that are beyond what is possible classically. However, quantum information is notoriously fragile. As decoherence sets the boundary between quantum and classical physics, noise can easily wash away any potential quantum advantage [14–16]. Quantum error correction [17–19] has been developed as a tool to combat noise in quantum computing, as well as in sensing and communication, yet it requires large-scale quantum processing with substantial resource overhead [20]. Despite the rapid progress of recent years, we are still at a stage where quantum devices have a relatively small number of qubits with limited control [21]. In this context, techniques of error mitigation are being developed, see e.g. Ref. [22, 23] and references therein. Though not necessarily scalable, these techniques aim at mitigating the harmful effects of noise on quantum information.

This work is inspired by a recently proposed approach known as superposed quantum error mitigation (SQEM), which exploits redundancy and constructive interference [24, 25]. Unlike other error mitigation schemes that are based on sampling or extrapolation, the approach considered here is based on hardware. Given a noisy quantum gate or circuit \mathcal{E} , SQEM is implemented by calling N i.i.d. instances of \mathcal{E} , which are applied in parallel to the input of the quantum computation and $N - 1$ auxiliary quantum systems. To harness inference, the N quantum systems are put in superposition by applying two control-swap gates, one before and one after the action of $\mathcal{E}^{\otimes N}$. Conditioned on successful measurements

of the control and auxiliary systems, Miguel-Ramiro et al. showed that SQEM may mitigate errors in the post-selected state, in principle up to unit fidelity at the cost of negligibly small probability of success.

Here we are interested in applications to astronomical imaging and communications, therefore an interferometric-based (IB) SQEM approach appears to be the most natural. We propose and explore in detail several explicit optical implementations and establish exact analytical results. We show that by using linear optics and vacuum modes one can improve tasks like entanglement distribution and stellar interferometry; errors can be mitigated up to near unit-fidelity with bounded resources and a finite probability of success. First, we present a scheme to distribute quantum coherence between distant laboratories, and show that IB SQEM can mitigate dephasing errors. Second, we discuss an application to boost the resolution of large-baseline telescopes without using quantum repeaters or quantum error correction [8, 26–28]. The scheme is effective against dephasing, but it does not enhance robustness to loss. The latter may be achieved by nesting IB SQEM with schemes robust to photon loss by design, e.g. [29]. Finally, we show how IB SQEM can be applied to distribute pairs of polarisation-entangled photons across a noisy channel, which is a fundamental task for quantum networks [30–33].

II. DISTRIBUTING COHERENCE

First, we consider distributing coherence among distant laboratories. The task is to distribute a single-photon state in superposition over two modes with a fixed relative phase. States of this form play an important role in dual-rail logic [34], fundamental quantum mechanics [35] and stellar interferometry [8]. Let $\{a_{A_0}^\dagger, a_{A_0}\}$ and

* cosmo.lupo@poliba.it

† zixin.huang@mq.edu.au

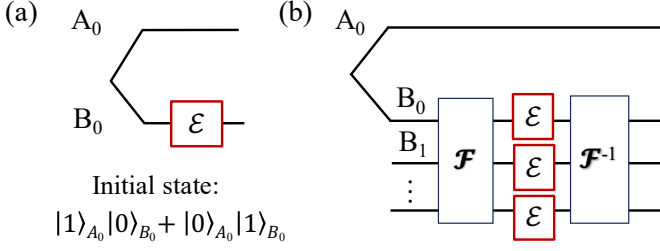


FIG. 1. Distribution of coherence, single-photon state over two modes, A_0 , B_0 , where noise is applied to the B modes: (a) no encoding is used, the quantum state is input into the channel directly. (b) IB SQEM is applied to mitigate noise on mode B_0 , using $N - 1$ vacuum ancillary modes, and a pair of N -port interferometers implementing the Fourier transform and its inverse.

$\{a_{B_0}^\dagger, a_{B_0}\}$ be the canonical bosonic creation and annihilation operators for the two modes. Consider the state

$$|\psi\rangle = \frac{1}{\sqrt{2}}(a_{A_0}^\dagger + a_{B_0}^\dagger)|0\rangle = \frac{1}{\sqrt{2}}(|10\rangle + |01\rangle), \quad (1)$$

where $|0\rangle$ is the vacuum, $|10\rangle \equiv |1\rangle_{A_0}|0\rangle_{B_0}$ represents the state of a photon in mode A_0 , and $|01\rangle \equiv |0\rangle_{A_0}|1\rangle_{B_0}$ that of a photon in mode B_0 . We want to distribute such a state to a distant laboratory by transmitting the mode B_0 through a noisy channel that induces dephasing. This is represented by the following map,

$$|\psi\rangle \rightarrow \mathcal{E}(|\psi\rangle\langle\psi|) = \int d\mu_\theta U_\theta |\psi\rangle\langle\psi| U_\theta^\dagger, \quad (2)$$

where

$$U_\theta |\psi\rangle = \frac{1}{\sqrt{2}}(|10\rangle + e^{i\theta}|01\rangle), \quad (3)$$

for some measure $d\mu_\theta$. We can readily compute the fidelity

$$F_1 = \langle\psi|\mathcal{E}(|\psi\rangle\langle\psi|)|\psi\rangle = \frac{1}{2}(1 + \text{Re}\{\kappa\}), \quad (4)$$

where

$$\kappa := \int d\mu_\theta e^{i\theta} = \mathbb{E}_\theta[e^{i\theta}]. \quad (5)$$

We now show that by using vacuum ancillary modes and linear optics, we achieve a partial cancellation of the noise, resulting in increased fidelity. To gain some intuition, we illustrate an example by using a single ancillary vacuum mode. The ancillary mode, denoted B_1 is initially prepared in the vacuum state, then mixed with mode B_0 at a 50/50 beam splitter. The action of the beam splitter on the state of a single photon over two

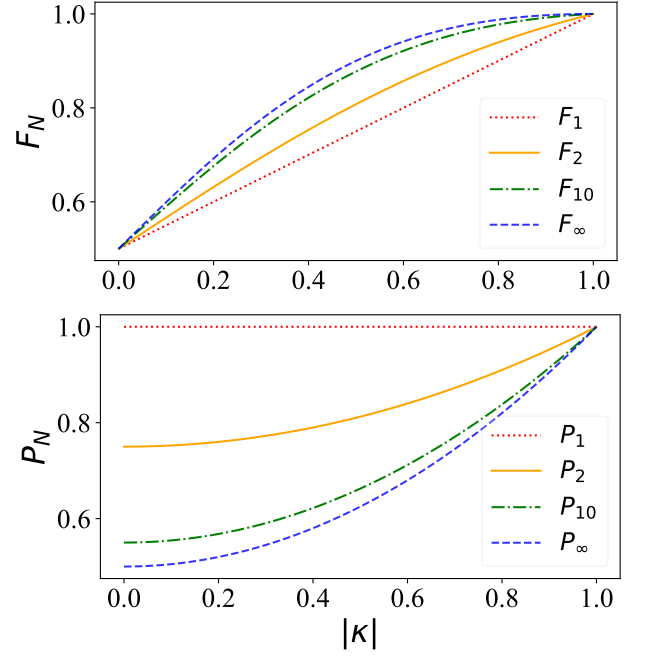


FIG. 2. Figures of merit for distribution of quantum coherence, when only the B modes are subject to dephasing noise (Fig. 1), assuming $\text{Im}\{\kappa\} = 0$. Top panel: fidelity F_N versus a function of the noise parameter $|\kappa|$, computed from Eq. (18); we show $N = 1, 2, 10$, and in the limit that $N \rightarrow \infty$. Bottom panel: post-selection probability P_N versus the noise parameter $|\kappa|$, computed from Eq. (17); from top to bottom for $N = 1, 2, 10$, and in the limit that $N \rightarrow \infty$.

modes is represented by a Hadamard gate, yielding

$$|\psi'\rangle = \frac{1}{\sqrt{2}}\left(|100\rangle + \frac{1}{\sqrt{2}}|010\rangle + \frac{1}{\sqrt{2}}|001\rangle\right), \quad (6)$$

where $|lmn\rangle \equiv |l\rangle_{A_0}|m\rangle_{B_0}|n\rangle_{B_1}$ represents the state of a single-photon over three modes. We assume that the modes B_0 and B_1 are affected by i.i.d. dephasing noise; for example, the two modes may travel through identical but uncoupled optical fibres. For each value of the local phase shifts we have

$$U_{\theta_1} \otimes U_{\theta_2} |\psi'\rangle = \frac{1}{\sqrt{2}}\left(|100\rangle + \frac{e^{i\theta_1}}{\sqrt{2}}|010\rangle + \frac{e^{i\theta_2}}{\sqrt{2}}|001\rangle\right). \quad (7)$$

Finally, the modes are interfered again at a 50/50 beam splitter, which accounts for applying a second Hadamard gate. Post-selecting on measuring the vacuum state on the auxiliary mode B_1 we obtain the following (unnormalised) state on signal modes A_0B_0

$$|\psi_{\theta_1\theta_2}\rangle = \frac{1}{\sqrt{2}}\left(|10\rangle + \frac{e^{i\theta_1} + e^{i\theta_2}}{2}|01\rangle\right). \quad (8)$$

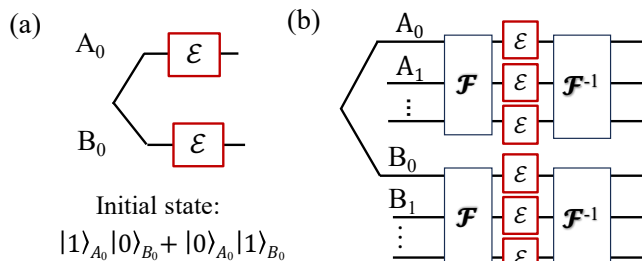


FIG. 3. Distribution of coherence, single-photon state over two modes, A_0 , B_0 , where noise is applied independently to A modes and B modes: (a) no encoding is used, the quantum state is input into the channel directly. (b) IB SQEM is applied to mitigate noise on modes A_0 and B_0 , using $2(N-1)$ vacuum ancillary modes, and four N -port interferometers implementing the Fourier transform and its inverse.

It remains to check that this state has fidelity larger than F_1 , hence noise is effectively reduced. We can anticipate that this is the case by inspection of Eq. (8), where the noise factor appears to be the average of two independent random variables, therefore its variance is half the variance of $e^{i\theta_1}$ and $e^{i\theta_2}$. By averaging over the random phase shifts we obtain the (un-normalised) state

$$\rho_2 = \int d\mu_{\theta_1} d\mu_{\theta_2} |\psi_{\theta_1\theta_2}\rangle \langle \psi_{\theta_1\theta_2}| \quad (9)$$

$$= \frac{1}{2} \left(|10\rangle \langle 10| + \frac{1+|\kappa|^2}{2} |01\rangle \langle 01| + \kappa |01\rangle \langle 10| + \text{h.c.} \right). \quad (10)$$

The probability that the photon arrives at mode B_0 is

$$P_2 = \text{Tr} \rho_2 = \frac{1}{2} \left(1 + \frac{1+|\kappa|^2}{2} \right), \quad (11)$$

from which we finally obtain the fidelity

$$F_2 = \frac{\langle \psi | \rho_2 | \psi \rangle}{P_2} = \frac{1}{2} \left(1 + \frac{4 \text{Re}\{\kappa\}}{3+|\kappa|^2} \right), \quad (12)$$

which is strictly greater than F_1 in Eq. (4) for any $|\kappa| \in (0, 1)$.

We can extend the protocol to $N-1$ ancillary modes, B_1, B_2, \dots, B_{N-1} . The ancillae are still prepared in the vacuum state, but the 50/50 beam splitter is replaced by a N -mode interferometer. For example, we can choose one that implements the Fourier transform, with matrix elements

$$\mathcal{F}_{hk} = \frac{1}{\sqrt{N}} e^{i2\pi hk/N}, \quad (13)$$

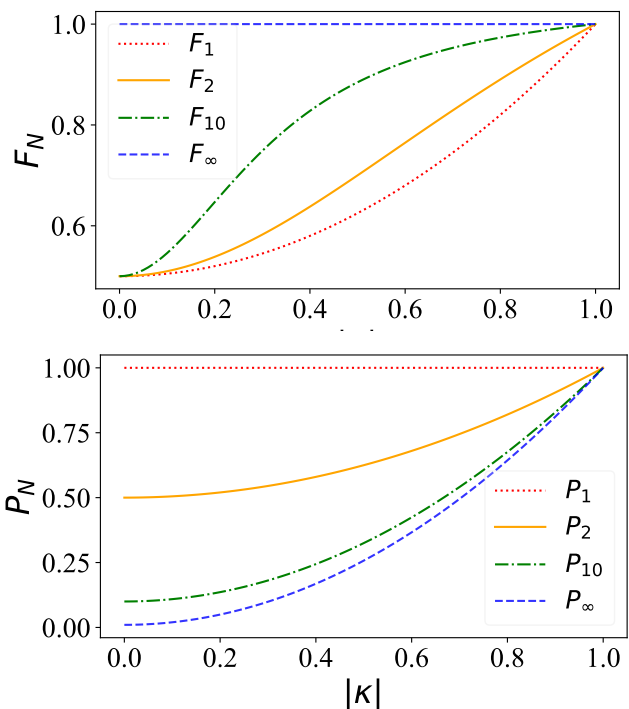


FIG. 4. Figures of merit of IB SQEM for distribution of quantum coherence, when both A modes and B modes are subject to dephasing noise. Top panel: fidelity F_N versus the noise parameter $|\kappa|$, computed from Eq. (21), showing $N = 1, 2, 10$, and in the limit that $N \rightarrow \infty$. Bottom panel: post-selection probability P_N versus the noise parameter $|\kappa|$, computed from Eq. (22), showing $N = 1, 2, 10$, and in the limit that $N \rightarrow \infty$. For example, with 9 ancillary modes we can improve the fidelity from 0.82 to 0.97 with a probability of success of about 68%.

for $h, k = 0, 1, \dots, N-1$. After the action of N i.i.d. dephasing channels, we apply the inverse Fourier transform,

$$[\mathcal{F}^\dagger]_{hk} = \frac{1}{\sqrt{N}} e^{-i2\pi hk/N}. \quad (14)$$

This is shown in Fig. 1.

The final state, post-selected on no photon arriving on the auxiliary modes, is described by the un-normalised state

$$|\psi_{\theta_1 \dots \theta_N}\rangle = \frac{1}{\sqrt{2}} \left(|10\rangle + |01\rangle \sum_{k=0}^{N-1} \frac{e^{i\theta_k}}{N} \right). \quad (15)$$

Note that here we have the average of N i.i.d. random variables, therefore we expect an N -fold reduction in the noise variance. Averaging over noise realisations

we obtain the post-selected state, which reads

$$\rho_N = \frac{1}{2} \left(|10\rangle\langle 10| + \frac{1 + (N-1)|\kappa|^2}{N} |01\rangle\langle 01| + \kappa |01\rangle\langle 10| + \text{h.c.} \right), \quad (16)$$

from which we obtain the post-selection probability

$$P_N = \frac{1}{2} \left(1 + \frac{1 + (N-1)|\kappa|^2}{N} \right) \quad (17)$$

and the fidelity

$$F_N = \frac{1}{2} \left(1 + \frac{2N \text{Re}\{\kappa\}}{1 + N + (N-1)|\kappa|^2} \right). \quad (18)$$

Note that the fidelity is monotonically increasing with N , while the post-selection probability decreases. Eventually, they approach limiting values

$$F_\infty = \frac{1}{2} \left(1 + \frac{2 \text{Re}\{\kappa\}}{1 + |\kappa|^2} \right), \quad (19)$$

$$P_\infty = \frac{1}{2} (1 + |\kappa|^2). \quad (20)$$

The fidelity is improved compared to the un-encoded case in Eq. (4) for all values of the noise parameter κ . We plot F_N and P_N in Fig. 2 as a function of $|\kappa|$ assuming $\text{Im}\{\kappa\} = 0$. The post-selection probability here is always larger than 1/2, since there is a 50% probability that the photon stays on mode A_0 , which is noiseless.

If we assume that mode A_0 is also affected by i.i.d. dephasing noise (Fig. 3), the post-selection probability may drop below 1/2. However, in this symmetric case, if IB SQEM is applied to modes A_0 and B_0 independently, with the help of $2(N-1)$ vacuum modes, then the fidelity and post-selection probability read

$$F_N^{\text{sym}} = \frac{1}{2} \left(1 + \frac{N|\kappa|^2}{1 + (N-1)|\kappa|^2} \right), \quad (21)$$

$$P_N^{\text{sym}} = |\kappa|^2 + \frac{1 - |\kappa|^2}{N}. \quad (22)$$

This shows that by increasing N the fidelity approaches one, while the post-selection probability remains above $|\kappa|^2$. These quantities are plotted in Fig. 4. As an example, with 9 ancillary modes we can improve the fidelity from 0.82 to 0.97 with a probability of success of about 68%.

III. ROBUSTNESS TO LOSS AND NOISE IN THE INTERFEROMETER

While the IB SQEM scheme partially cancels dephasing noise, it is not able to mitigate loss. However, since there is only one photon travelling in the interferometer,

the fidelity in Eq. (18) still holds conditioned on the event that the photon is not lost. In other words, the overall loss is not affected by introducing auxiliary modes. If each branch of the interferometer has an equal attenuation factor η , then the state in Eq. (15) is replaced by

$$|\psi_{\eta; \theta_1 \dots \theta_N}\rangle = \frac{1}{\sqrt{2}} \left(|10\rangle + \sqrt{\eta} \sum_{k=0}^{N-1} \frac{e^{i\theta_k}}{N} |01\rangle \right), \quad (23)$$

and the fidelity reads

$$F_N^\eta = \frac{1}{2} \left(1 + \frac{2N\sqrt{\eta} \text{Re}\{\kappa\}}{\eta + N + \eta(N-1)|\kappa|^2} \right). \quad (24)$$

While the scheme is not able to mitigate loss, it does not introduce extra losses because the path length that the photons travel through remains the same. To achieve resilience to both dephasing and loss, IB SQEM may be nested with protocols that are robust to loss by design, e.g. Ref. [29].

Most importantly, in practice, introducing an N -mode interferometer will inevitably add loss and noise to the system. To model additional dephasing, we assume that the dephasing noise in each branch of the interferometer is i.i.d. and quantified by the parameter $\tilde{\kappa} > \kappa$, where in principle $\tilde{\kappa}$ may depend on N . Also, we assume that the interferometer introduces loss with an overall attenuation factor η . Within this model, IB SQEM is still capable of enhancing fidelity as long as

$$\frac{2N\sqrt{\eta} \text{Re}\{\tilde{\kappa}\}}{\eta + N + \eta(N-1)|\tilde{\kappa}|^2} > \text{Re}\{\kappa\}. \quad (25)$$

IV. STELLAR INTERFEROMETRY

In the context of quantum-enhanced telescopes [8], consider the task of stellar interferometry in a two-site scenario, telescope station A and telescope station B , separated by large distances. One of the main challenges for realising a long-baseline interferometer is phase stabilisation, where thermal fluctuation leads to uncertainty in the path length of a fibre [36], which can degrade the signals.

In the weak-signal limit [8, 26, 28, 37], we model the stellar state as a single photon is received by either of the two telescopes. This is described by

$$|\psi_\phi\rangle = \frac{1}{\sqrt{2}} (|10\rangle + e^{i\phi} |01\rangle), \quad (26)$$

where the relative phase ϕ is due to the difference in path length between the source and the telescope sites. It encodes information about the location of stellar sources. One task in stellar interferometry is to estimate optimally the parameter ϕ . As a figure of merit, we use the quantum Fisher information (QFI), which bounds

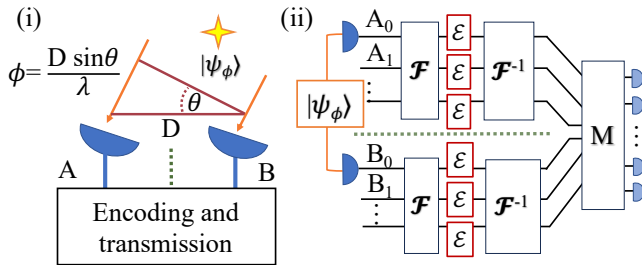


FIG. 5. Application to stellar interferometry: (i) Light is collected at two sites, A and B that are spatially separated. (ii) To mitigate phase noise, ancillary vacuum modes are introduced locally; before transmission, modes A and B are encoded using a N -port interferometer implementing the Fourier transform \mathcal{F} , after the transmission, the inverse Fourier transform \mathcal{F}^{-1} is applied before measurement.

the inverse of the statistical error variance per photon received [38, 39]. See Ref. [38] for a review of the QFI.

As local measurements would not allow us to achieve this goal, we need to send light collected by the distant telescopes towards a common measurement station, where the two paths are interfered. We assume that the measurement station is exactly in the middle between the two telescopes. En route from the telescopes to the measurement station, modes A_0 and B_0 are affected by i.i.d. dephasing noise, as in the symmetric case discussed above. The density matrix of the state at the output of the noisy channel is

$$\rho_{\phi;1} = \frac{1}{2} (|10\rangle\langle 10| + |01\rangle\langle 01| + e^{i\phi}|\kappa|^2 |10\rangle\langle 01| + \text{h.c.}), \quad (27)$$

the QFI of the parameter ϕ in Eq. (27) is [40],

$$I_Q^{(1)} = |\kappa|^4. \quad (28)$$

We now show that IB SQEM can yield up to a quadratic factor of improvement in the QFI in terms of κ . Due to the operational meaning of the QFI, and for a fair comparison, we will consider the QFI of the average state and do not post-select. Since we have assumed the measurement station to be in the middle, we apply IB SQEM to both noisy modes A_0 and B_0 . Therefore, in the simplest setup, we introduce ancillary modes A_1 and B_1 . Hadarmard gates (i.e. 50/50 beam splitters) couple mode A_0 with A_1 and, independently, mode B_0 with B_1 , yielding

$$|\psi_\phi\rangle \rightarrow \frac{1}{2} (|10; 00\rangle + |01; 00\rangle + e^{i\phi} |00; 10\rangle + e^{i\phi} |00; 01\rangle), \quad (29)$$

where $|lm; np\rangle \equiv |l\rangle_{A_0}|m\rangle_{A_1}|n\rangle_{B_0}|p\rangle_{B_1}$. After passing through the dephasing channels, every off-diagonal component will pick up the factor $|\kappa|^2$,

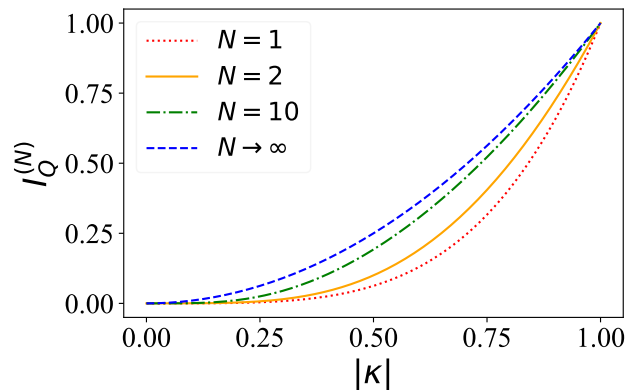


FIG. 6. The plot shows the QFI for the estimation of the phase ϕ , plotted against the noise parameter $|\kappa|$. The QFI is computed using Eq. (38). We show $N = 1, 2, 10$ and in the limit that $N \rightarrow \infty$.

therefore the density matrix, expressed in the basis $\{|10; 00\rangle, |01; 00\rangle, |00; 10\rangle, |00; 01\rangle\}$, reads

$$\frac{1}{4} \begin{pmatrix} 1 & |\kappa|^2 & e^{-i\phi}|\kappa|^2 & e^{-i\phi}|\kappa|^2 \\ |\kappa|^2 & 1 & e^{-i\phi}|\kappa|^2 & e^{-i\phi}|\kappa|^2 \\ e^{i\phi}|\kappa|^2 & e^{i\phi}|\kappa|^2 & 1 & |\kappa|^2 \\ e^{i\phi}|\kappa|^2 & e^{i\phi}|\kappa|^2 & |\kappa|^2 & 1 \end{pmatrix}. \quad (30)$$

Finally, this state is passed through another pair of independent Hadamard gates, yielding

$$\rho_{\phi;2} = \frac{1}{2} \begin{pmatrix} \frac{1+|\kappa|^2}{2} & 0 & e^{-i\phi}|\kappa|^2 & 0 \\ 0 & \frac{1-|\kappa|^2}{2} & 0 & 0 \\ e^{i\phi}|\kappa|^2 & 0 & \frac{1+|\kappa|^2}{2} & 0 \\ 0 & 0 & 0 & \frac{1-|\kappa|^2}{2} \end{pmatrix}. \quad (31)$$

This shows that the photon appears in modes A_0B_0 with probability P_2^{sym} from Eq. (22), carrying the phase ϕ . The state of the photon on modes A_0B_0 is equivalent to Eq. (27) upon replacing κ with κ_2 , where

$$|\kappa_2|^2 = \frac{2|\kappa|^2}{1 + |\kappa|^2}. \quad (32)$$

Otherwise, if the photon ends in modes A_1B_1 , it bears no phase information. Therefore, using Eq. (28) we obtain the expression for the QFI,

$$I_Q^{(2)} = P_2^{\text{sym}} |\kappa_2|^4 = \frac{2|\kappa|^4}{1 + |\kappa|^2}, \quad (33)$$

which is larger than $I_Q^{(1)}$ for any $|\kappa| \in (0, 1)$.

We now extend this result to the general case of $2(N-1)$ ancillary modes. First, each group of N modes is passed through an N -port interferometer implementing the Fourier transform. Then, we apply the local i.i.d. noise on each mode. The resulting density matrix

has a block diagonal form, which generalises Eq. (30),

$$\rho_{\phi;N} = \begin{pmatrix} C & D \\ D^* & C \end{pmatrix} \quad (34)$$

where C has 1's along the main diagonal and the other elements are proportional to $|\kappa|^2$,

$$C \equiv \frac{1}{2N} \begin{pmatrix} 1 & |\kappa|^2 & \cdots & |\kappa|^2 \\ |\kappa|^2 & 1 & \ddots & \vdots \\ \vdots & \ddots & \ddots & \vdots \\ |\kappa|^2 & |\kappa|^2 & \cdots & 1 \end{pmatrix}, \quad (35)$$

and D has all elements equal

$$D \equiv \frac{e^{i\phi}|\kappa|^2}{2N} \begin{pmatrix} 1 & 1 & \cdots & 1 \\ 1 & 1 & \cdots & \vdots \\ \vdots & \vdots & \ddots & \vdots \\ 1 & 1 & \cdots & 1 \end{pmatrix}. \quad (36)$$

Note that the Fourier transform diagonalises both C and D , yielding a state $\rho_{\phi;N}$ with a similar form to the state in Eq. (31). In particular, the phase information is carried only by the photon appearing on modes A_0B_0 after \mathcal{F}^{-1} is applied. This occurs with probability P_N^{sym} as in Eq. (22). Then, κ is effectively replaced by κ_N , with

$$|\kappa_N|^2 = \frac{N|\kappa|^2}{1 + (N-1)|\kappa|^2}. \quad (37)$$

Finally, using again Eq. (28) we obtain

$$I_Q^{(N)} = P_N^{\text{sym}}|\kappa_N|^2 = \frac{N|\kappa|^4}{1 + (N-1)|\kappa|^2}. \quad (38)$$

In the limit that $N \rightarrow \infty$, we have $I_Q^N \rightarrow |\kappa|^2$, i.e. we gain a quadratic factor in $|\kappa|$ in the QFI. We plot the QFI for $N = 1, 2, 10$ and $N \rightarrow \infty$ in Fig. 6. We see that there is a notable gap for all values of $|\kappa|$, and the QFI monotonically increases by increasing the number of auxiliary modes.

V. DISTRIBUTING ENTANGLEMENT

Entanglement distribution is arguably one of the most important primitives for quantum networks, it is the one that enables quantum repeaters and device-independent quantum key distribution [31]. Consider a maximally entangled state of two photons in polarisation:

$$|\psi\rangle = \frac{1}{\sqrt{2}} (|HH\rangle + |VV\rangle), \quad (39)$$

where $|HH\rangle$ and $|VV\rangle$ represent two photons with either horizontal or vertical polarisation. Let the second photon

travel through a noisy communication channel. To model this noise, we consider a random unitary channel acting on the second qubit. This model is rather general (but it does not account for loss). We represent such a channel as follows:

$$|\psi\rangle \rightarrow \int d\mu_{\mathbf{r}} (I \otimes U) |\psi\rangle \langle \psi| (I \otimes U^\dagger), \quad (40)$$

where

$$U = e^{i\mathbf{r} \cdot \boldsymbol{\sigma}} = (\cos |\mathbf{r}|) \mathbb{I}_2 + i \frac{\mathbf{r}}{|\mathbf{r}|} \cdot \boldsymbol{\sigma} \sin |\mathbf{r}|. \quad (41)$$

Here \mathbf{r} is a random vector, \mathbb{I}_2 is the identity matrix, and $\boldsymbol{\sigma} = (X, Y, Z)$ is the vector of Pauli matrices. For any measure $d\mu_{\mathbf{r}}$, this is a representation of a generic Pauli channel. For each realisation of the noise parameter \mathbf{r} , the state is transformed as follows,

$$|\psi\rangle \rightarrow \frac{1}{\sqrt{2}} (|H\rangle U |H\rangle + |V\rangle U |V\rangle), \quad (42)$$

from which we obtain the entanglement fidelity after averaging over the noise realisations,

$$F_1 = \frac{1}{4} \int d\mu_{\mathbf{r}} |\langle H|U|H\rangle + \langle V|U|V\rangle|^2 \quad (43)$$

$$= \frac{1}{4} \int d\mu_{\mathbf{r}} |\text{Tr}U|^2 = \mathbb{E}_{\mathbf{r}}[(\cos |\mathbf{r}|)^2]. \quad (44)$$

We now discuss how to implement IB SQEM with $N-1$ ancillary modes for the task of entanglement distribution. To do that we need to introduce an N -dimensional space, spanned by the basis vectors $\{|0\rangle, |1\rangle, \dots, |N\rangle\}$ that accounts for the degrees of freedom of the interferometer, which for example may be spatial degrees of freedom. Formally, these external degrees of freedom are combined with the internal degrees of freedom of polarisation by tensor product. Initially, the signal is in the first external mode (labelled as 0), therefore we rewrite (39) as

$$|\psi\rangle = \frac{1}{\sqrt{2}} (|H\rangle|H\rangle + |V\rangle|V\rangle) |0\rangle. \quad (45)$$

First, the state passes through an N -mode interferometer that implements the Fourier transform:

$$|\psi\rangle \rightarrow \frac{1}{\sqrt{2}} (|H\rangle|H\rangle + |V\rangle|V\rangle) \frac{\sum_{k=0}^{N-1} |k\rangle}{\sqrt{N}}. \quad (46)$$

Each branch of the interferometer is affected by i.i.d. noise, which formally is a control-unitary:

$$|\psi\rangle \rightarrow \frac{1}{\sqrt{2N}} \sum_{k=0}^{N-1} (|H\rangle U_k |H\rangle + |V\rangle U_k |V\rangle) |k\rangle. \quad (47)$$

Finally, the inverse Fourier transform is applied. We post-select on the event that no photon arrives in the

ancillary modes, obtaining the un-normalised state

$$\frac{1}{\sqrt{2}} \left(|H\rangle \sum_{k=0}^{N-1} \frac{U_k}{N} |H\rangle + |V\rangle \sum_{k=0}^{N-1} \frac{U_k}{N} |V\rangle \right). \quad (48)$$

The norm of this vector, after averaging over the noise realisation, gives the post-selection probability,

$$P_N = \frac{1}{2} \int \prod_j d\mu_{r_j} \text{Tr} \left(\frac{\sum_k U_k^\dagger \sum_{k'} U_{k'}}{N} \right) \quad (49)$$

$$= \frac{1}{2} \int \prod_j d\mu_{r_j} \text{Tr} \left(\frac{N\mathbb{I} + \sum_{k \neq k'} U_k^\dagger U_{k'}}{N^2} \right) \quad (50)$$

$$= \frac{1}{N} + \frac{N-1}{2N} \text{Tr} (\mathbb{E}_{\mathbf{r}} [U^\dagger] \mathbb{E}_{\mathbf{r}} [U]). \quad (51)$$

To simplify the notation we assume that the noise distribution is symmetric, i.e.,

$$\mathbb{E}_{\mathbf{r}} [U] = \mathbb{E}_{\mathbf{r}} [\cos |\mathbf{r}|] \mathbb{I}_2. \quad (52)$$

With this assumption we obtain

$$P_N = \frac{1}{N} (1 + (N-1) \mathbb{E}[\cos^2 |\mathbf{r}|]). \quad (53)$$

Similarly, the entanglement fidelity reads

$$F_N = \frac{1}{4P_N} \int \prod_j d\mu_{r_j} \left| \text{Tr} \sum_{k=0}^{N-1} \frac{U_k}{N} \right|^2 \quad (54)$$

$$= \frac{1}{4P_N} \frac{\mathbb{E}_{\mathbf{r}} [|\text{Tr} U|^2] + (N-1) \mathbb{E}_{\mathbf{r}} [\text{Tr} U^\dagger] \mathbb{E}_{\mathbf{r}} [\text{Tr} U]}{N} \quad (55)$$

$$= \frac{1}{P_N} \frac{\mathbb{E}_{\mathbf{r}} [(\cos |\mathbf{r}|)^2] + (N-1) \mathbb{E}_{\mathbf{r}} [(\cos |\mathbf{r}|)]^2}{N}, \quad (56)$$

which for symmetric noise simplifies to

$$F_N = \frac{\mathbb{E}[(\cos |\mathbf{r}|)^2] + (N-1) \mathbb{E}[(\cos |\mathbf{r}|)]^2}{1 + (N-1) \mathbb{E}[\cos^2 |\mathbf{r}|]}. \quad (57)$$

Note that the entanglement fidelity tends to one by increasing N , irrespective of the noise strength, yet the probability of success remains always larger than $\mathbb{E}[\cos^2 |\mathbf{r}|]$.

As an example, consider a Gaussian distributed noise, such that $d\mu_{|\mathbf{r}|}$ is proportional to $e^{-|\mathbf{r}|^2/2\sigma^2}$. We obtain

$$\mathbb{E}[\cos |\mathbf{r}|] = e^{-\sigma^2/2}, \quad (58)$$

$$\mathbb{E}[(\cos |\mathbf{r}|)^2] = e^{-\sigma^2} \cosh \sigma^2. \quad (59)$$

The entanglement fidelity for this model is plotted in Fig. 7 together with the post-selection probability. The numerical example in the figure shows that with 9 vacuum ancillae one may boost the entanglement fidelity from 0.80 to 0.97 with a probability of success above 80%.

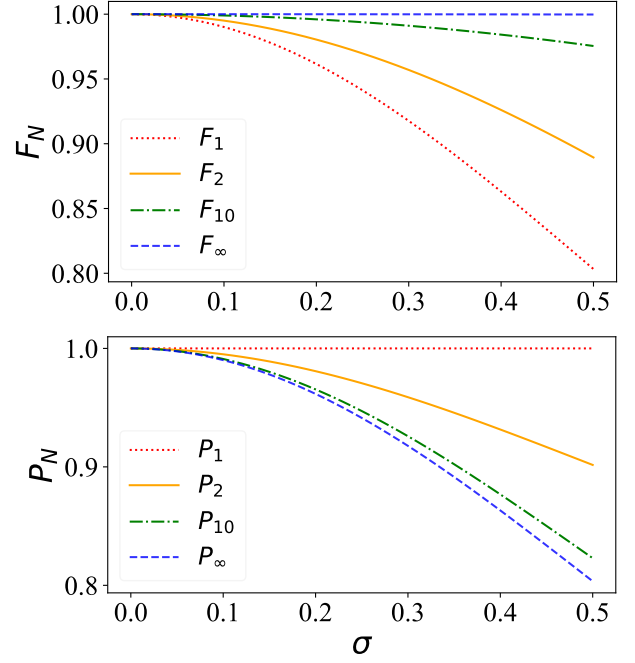


FIG. 7. Figures of merit for entanglement distribution, for the Gaussian noise model in Eqs. (58)-(59). Top figure: entanglement fidelity F_N versus the noise parameter σ , computed from Eq. (57); from bottom to top for $N = 1, 2, 10$, and in the limit that $N \rightarrow \infty$. Bottom figure: post-selection probability P_N versus the noise parameter σ , computed from Eq. (53); from top to bottom for $N = 1, 2, 10$, and in the limit that $N \rightarrow \infty$. For example, by using 9 ancillary modes, we can improve the fidelity from 0.80 to 0.97 with probability of success above 80%.

VI. CONCLUSIONS

We have proposed to use interferometry to mitigate dephasing noise that afflicts photonic quantum information carriers. We have discussed applications to preserve coherence in single-photon states, to stabilise the phase in stellar interferometry, and to improve entanglement distribution. Our scheme uses only passive linear optics and vacuum ancillary modes, without the need for ancillary entanglement or optical non-linearity. For coherence and entanglement distribution, the state can be preserved up to near unit-fidelity, with a finite probability of success. In stellar interferometry, we show that the Quantum Fisher information can be increased by up to a quadratic factor.

The optimal performance of our scheme is achieved asymptotically for a large number of auxiliary modes, which means bying an interferometer with many input ports. However, in most cases a relatively low number of modes is sufficient to approximate the asymptotic performance. For example, the plots in Figs. (2), (6), (7) suggest that a ten-mode interferometer already yields near-optimal results even for strong noise. For weak noise an even smaller interferometer may suffice.

In practice, the introduction of a multi-mode interferometer will necessarily increase the complexity of the experimental apparatus, possibly introducing additional sources of loss and noise. This is an important point for the experimental viability of our scheme. Nevertheless, our initial analysis suggests that the error mitigation scheme possesses some degree of robustness to extra dephasing due to the interferometer. For what concern increased loss, for protocols involving only single-photon states, this is expected to reduce the probability of success without essentially reducing the fidelity. Our protocol is most naturally implemented on integrated photonic circuits, and given the recent experimental progress, where research groups globally have demonstrated chips that are reconfigurable [41], high-fidelity [42–44] and high-transmission [45], we expect our protocol to become a viable way to combat dephasing noise, paving a pathway to the practical application of quantum technology.

VII. ACKNOWLEDGEMENTS

This work has received support from: Italian Space Agency, project ‘Subdiffraction Quantum Imaging’ (SQI) n. 2023-13-HH.0; European Union, Next Generation EU: PNR MUR project PE0000023-NQSTI; and Horizon Europe research and innovation programme under the project ‘Quantum Secure Networks Partnership’ (QSNP, grant agreement No. 101114043). ZH thanks the generous hospitality of UTS:QSI during which this work was carried out and thanks Ryan Mann for discussions. ZH is supported by a Sydney Quantum Academy Postdoctoral Fellowship .

-
- [1] P. Shor, Algorithms for quantum computation: discrete logarithms and factoring, in *Proceedings 35th Annual Symposium on Foundations of Computer Science* (1994) pp. 124–134.
- [2] L. K. Grover, A fast quantum mechanical algorithm for database search, in *Proceedings of the Twenty-Eighth Annual ACM Symposium on Theory of Computing*, STOC ’96 (Association for Computing Machinery, New York, NY, USA, 1996) p. 212–219.
- [3] S. McArdle, S. Endo, A. Aspuru-Guzik, S. C. Benjamin, and X. Yuan, Quantum computational chemistry, *Rev. Mod. Phys.* **92**, 015003 (2020).
- [4] M. C. Bañuls, R. Blatt, J. Catani, A. Celi, J. I. Cirac, M. Dalmonte, L. Fallani, K. Jansen, M. Lewenstein, S. Montangero, C. A. Muschik, B. Reznik, E. Rico, L. Tagliacozzo, K. V. Acoleyen, F. Verstraete, U.-J. Wiese, M. Wingate, J. Zakrzewski, and P. Zoller, Simulating lattice gauge theories within quantum technologies, *Eur. Phys. J. D* **74**, 165 (2020).
- [5] A. D. Meglio, K. Jansen, I. Tavernelli, C. Alexandrou, S. Arunachalam, C. W. Bauer, K. Borrás, S. Carrazza, A. Crippa, V. Croft, R. de Putter, A. Delgado, V. Dunjko, D. J. Egger, E. Fernandez-Combarro, E. Fuchs, L. Funcke, D. Gonzalez-Cuadra, M. Grossi, J. C. Halimeh, Z. Holmes, S. Kuhn, D. Lacroix, R. Lewis, D. Lucchesi, M. L. Martinez, F. Meloni, A. Mezzacapo, S. Montangero, L. Nagano, V. Radescu, E. R. Ortega, A. Roggero, J. Schuhmacher, J. Seixas, P. Silvi, P. Spentzouris, F. Tacchino, K. Temme, K. Terashi, J. Tura, C. Tuysuz, S. Vallecorsa, U.-J. Wiese, S. Yoo, and J. Zhang, Quantum computing for high-energy physics: State of the art and challenges. summary of the qc4hep working group, arXiv preprint arXiv:2307.03236 (2023).
- [6] A. N. Boto, P. Kok, D. S. Abrams, S. L. Braunstein, C. P. Williams, and J. P. Dowling, Quantum interferometric optical lithography: Exploiting entanglement to beat the diffraction limit, *Phys. Rev. Lett.* **85**, 2733 (2000).
- [7] J. P. Dowling, Quantum optical metrology – the low-down on high-n00n states, *Contemporary Physics* **49**, 125 (2008), <https://doi.org/10.1080/00107510802091298>.
- [8] D. Gottesman, T. Jennewein, and S. Croke, Longer-baseline telescopes using quantum repeaters, *Phys. Rev. Lett.* **109**, 070503 (2012).
- [9] M. Tsang, R. Nair, and X.-M. Lu, Quantum theory of superresolution for two incoherent optical point sources, *Phys. Rev. X* **6**, 031033 (2016).
- [10] C. L. Degen, F. Reinhard, and P. Cappellaro, Quantum sensing, *Rev. Mod. Phys.* **89**, 035002 (2017).
- [11] C. H. Bennett and G. Brassard, Quantum cryptography: Public key distribution and coin tossing, *Proceedings of the IEEE International Conference on Computers, Systems and Signal Processing*, Bangalore, India, 10–12 December, 1984 **175**, 8 (1984).
- [12] A. K. Ekert, Quantum cryptography based on bell’s theorem, *Phys. Rev. Lett.* **67**, 661 (1991).
- [13] A. Acín, N. Brunner, N. Gisin, S. Massar, S. Pironio, and V. Scarani, Device-independent security of quantum cryptography against collective attacks, *Phys. Rev. Lett.* **98**, 230501 (2007).
- [14] M. J. Bremner, A. Montanaro, and D. J. Shepherd, Achieving quantum supremacy with sparse and noisy commuting quantum computations, *Quantum* **1**, 8 (2017).
- [15] K. Noh, L. Jiang, and B. Fefferman, Efficient classical simulation of noisy random quantum circuits in one dimension, *Quantum* **4**, 318 (2020).
- [16] D. Aharonov, X. Gao, Z. Landau, Y. Liu, and U. Vazirani, A polynomial-time classical algorithm for noisy random circuit sampling, in *Proceedings of the 55th Annual ACM Symposium on Theory of Computing* (2023) pp. 945–957.
- [17] B. M. Terhal, Quantum error correction for quantum memories, *Rev. Mod. Phys.* **87**, 307 (2015).
- [18] J. Roffe, Quantum error correction: an introductory guide, *Contemporary Physics* **60**, 226 (2019).
- [19] S. J. Devitt, W. J. Munro, and K. Nemoto, Quantum error correction for beginners, *Reports on Progress in Physics* **76**, 076001 (2013).

- [20] E. T. Campbell, B. M. Terhal, and C. Vuillot, Roads towards fault-tolerant universal quantum computation, *Nature* **549**, 172 (2017).
- [21] J. Preskill, Quantum computing in the nisq era and beyond, *Quantum* **2**, 79 (2018).
- [22] D. Bultrini, M. H. Gordon, P. Czarnik, A. Arrasmith, M. Cerezo, P. J. Coles, and L. Cincio, Unifying and benchmarking state-of-the-art quantum error mitigation techniques, *Quantum* **7**, 1034 (2023).
- [23] Z. Cai, R. Babbush, S. C. Benjamin, S. Endo, W. J. Huggins, Y. Li, J. R. McClean, and T. E. O’Brien, Quantum error mitigation, arXiv preprint arXiv:2210.00921 (2022).
- [24] J. Miguel-Ramiro, Z. Shi, L. Dellantonio, A. Chan, C. A. Muschik, and W. Dür, Sqem: Superposed quantum error mitigation, arXiv preprint arXiv:2304.08528 (2023).
- [25] J. Miguel-Ramiro, Z. Shi, L. Dellantonio, A. Chan, C. A. Muschik, and W. Dür, Enhancing quantum computation via superposition of quantum gates, arXiv preprint arXiv:2304.08529 (2023).
- [26] E. T. Khabiboulline, J. Borregaard, K. De Greve, and M. D. Lukin, Optical interferometry with quantum networks, *Phys. Rev. Lett.* **123**, 070504 (2019).
- [27] E. T. Khabiboulline, J. Borregaard, K. De Greve, and M. D. Lukin, Quantum-assisted telescope arrays, *Phys. Rev. A* **100**, 022316 (2019).
- [28] Z. Huang, G. K. Brennen, and Y. Ouyang, Imaging stars with quantum error correction, *Phys. Rev. Lett.* **129**, 210502 (2022).
- [29] M. M. Marchese and P. Kok, Large baseline optical imaging assisted by single photons and linear quantum optics, *Phys. Rev. Lett.* **130**, 160801 (2023).
- [30] H. J. Kimble, The quantum internet, *Nature* **453**, 1023 (2008).
- [31] S. Wehner, D. Elkouss, and R. Hanson, Quantum internet: A vision for the road ahead, *Science* **362**, eaam9288 (2018).
- [32] P. P. Rohde, *The quantum internet: The second quantum revolution* (Cambridge University Press, 2021).
- [33] Z. Huang, S. K. Joshi, D. Aktas, C. Lupo, A. O. Quintavalle, N. Venkatachalam, S. Wengerowsky, M. Lončarić, S. P. Neumann, B. Liu, *et al.*, Experimental implementation of secure anonymous protocols on an eight-user quantum key distribution network, *npj Quantum Information* **8**, 25 (2022).
- [34] P. Kok, W. J. Munro, K. Nemoto, T. C. Ralph, J. P. Dowling, and G. J. Milburn, Linear optical quantum computing with photonic qubits, *Rev. Mod. Phys.* **79**, 135 (2007).
- [35] S. M. Tan, D. F. Walls, and M. J. Collett, Nonlocality of a single photon, *Phys. Rev. Lett.* **66**, 252 (1991).
- [36] C. C.-W. Lim and C. Wang, Long-distance quantum key distribution gets real, *Nature Photonics* **15**, 554 (2021).
- [37] M. Tsang, Quantum nonlocality in weak-thermal-light interferometry, *Phys. Rev. Lett.* **107**, 270402 (2011).
- [38] M. G. A. Paris, Quantum estimation for quantum technology, *International Journal of Quantum Information* **07**, 125 (2009), <https://doi.org/10.1142/S0219749909004839>.
- [39] J. S. Sidhu and P. Kok, Geometric perspective on quantum parameter estimation, *AVS Quantum Science* **2**, 014701 (2020), <https://pubs.aip.org/avs/aqs/article-pdf/doi/10.1116/1.5119961/16700179/014701.1.online.pdf>.
- [40] Z. Huang, C. Macchiavello, and L. Maccone, Usefulness of entanglement-assisted quantum metrology, *Phys. Rev. A* **94**, 012101 (2016).
- [41] J. Notaros, J. Mower, M. Heuck, C. Lupo, N. C. Harris, G. R. Steinbrecher, D. Bunandar, T. Baehr-Jones, M. Hochberg, S. Lloyd, and D. Englund, Programmable dispersion on a photonic integrated circuit for classical and quantum applications, *Opt. Express* **25**, 21275 (2017).
- [42] A. Politi, J. C. Matthews, M. G. Thompson, and J. L. O’Brien, Integrated quantum photonics, *IEEE Journal of Selected Topics in Quantum Electronics* **15**, 1673 (2009).
- [43] J. Wang, S. Paesani, Y. Ding, R. Santagati, P. Skrzypczyk, A. Salavrakos, J. Tura, R. Augusiak, L. Mančinska, D. Bacco, *et al.*, Multidimensional quantum entanglement with large-scale integrated optics, *Science* **360**, 285 (2018).
- [44] G. Moody, V. J. Sorger, D. J. Blumenthal, P. W. Juodawlkis, W. Loh, C. Sorace-Agaskar, A. E. Jones, K. C. Balram, J. C. Matthews, A. Laing, *et al.*, 2022 roadmap on integrated quantum photonics, *Journal of Physics: Photonics* **4**, 012501 (2022).
- [45] H. Wang, J. Qin, X. Ding, M.-C. Chen, S. Chen, X. You, Y.-M. He, X. Jiang, L. You, Z. Wang, C. Schneider, J. J. Renema, S. Höfling, C.-Y. Lu, and J.-W. Pan, Boson sampling with 20 input photons and a 60-mode interferometer in a 10^{14} -dimensional hilbert space, *Phys. Rev. Lett.* **123**, 250503 (2019).

Appendix A: Direct interferometry

Consider a noisy quantum channel that induces dephasing

$$\rho \rightarrow \mathcal{E}(\rho) = \int d\theta \mu(\theta) U(\theta) \rho U(\theta)^\dagger, \quad \int d\theta \mu(\theta) = 1 \quad (\text{A1})$$

Assume each of the noise channel is narrow and Gaussian-distributed with variance σ^2 and centered at 0:

$$\mu(\theta) = \frac{1}{\sqrt{2\pi}\sigma} \exp\left[-\frac{1}{2}\left(\frac{\theta}{\sigma}\right)^2\right], \quad \sigma \ll 1. \quad (\text{A2})$$

In the weak-photon limit, a single photon is received by Alice and Bob at a time, which can be written as

$$|\psi_\phi\rangle = \frac{1}{\sqrt{2}} (|01\rangle_{A_0 B_0} + e^{i\phi} |10\rangle_{A_1 B_1}). \quad (\text{A3})$$

The corresponding density matrix is then

$$|\psi_\phi\rangle \langle\psi_\phi| = \frac{1}{2} (|01\rangle \langle 01| + e^{-i\phi} |01\rangle \langle 10| + e^{i\phi} |10\rangle \langle 01| + |10\rangle \langle 10|)_{A_0 B_0} \quad (\text{A4})$$

1. No encoding

Suppose we send the signal through the channel directly without encoding,

$$\rho_\phi \rightarrow \mathcal{E}_{A_0} \circ \mathcal{E}_{B_0} (|\psi_\phi\rangle \langle\psi_\phi|) \quad (\text{A5})$$

We now calculate this state explicitly

$$\begin{aligned} & \mathcal{E}_{A_0} \circ \mathcal{E}_{B_0} (|\psi_\phi\rangle \langle\psi_\phi|) (|\psi_\phi\rangle \langle\psi_\phi|) \\ &= \frac{1}{2} (|01\rangle \langle 01| + |10\rangle \langle 10|) + \frac{1}{2} \int d\theta d\theta' \mu_{A_1}(\theta) d\theta \mu_{B_1}(\theta') \left(e^{-i\phi} e^{i\theta} |01\rangle \langle 10| e^{\theta'} + e^{i\phi} e^{-i\theta} |10\rangle \langle 01| e^{i\theta'} \right) \\ &= \frac{1}{2} (|01\rangle \langle 01| + |10\rangle \langle 10|) + \frac{1}{2} \left(e^{-i\phi} e^{-\sigma^2} |01\rangle \langle 10| + e^{i\phi} e^{-\sigma^2} |10\rangle \langle 01| \right) \\ &\approx \frac{1}{2} (|01\rangle \langle 01| + |10\rangle \langle 10|) + (e^{-i\phi} |\kappa|^2 |01\rangle \langle 10| + e^{i\phi} |\kappa|^2 |10\rangle \langle 01|) \end{aligned} \quad (\text{A6})$$

where we have defined $\kappa = \int_{-\infty}^{\infty} e^{i\theta} \mu(\theta)$. This leads to

$$\rho_\phi = \frac{1}{2} (|01\rangle \langle 01| + |10\rangle \langle 10|) + \frac{1}{2} (e^{-i\phi} |\kappa|^2 |01\rangle \langle 10| + e^{i\phi} |\kappa|^2 |10\rangle \langle 01|) \quad (\text{A7})$$

For the state in Eq. A7, the QFI of the parameter ϕ is

$$I_Q = |\kappa|^4 \quad (\text{A8})$$

2. Two-mode encoding

Now let us look at the scenario where we use two modes, where the modes $A_0(B_0)$ is coupled to the mode $A_1(B_1)$ with the Hadamard gate

$$H = \frac{1}{\sqrt{2}} \begin{pmatrix} 1 & 1 \\ 1 & -1 \end{pmatrix} \quad (\text{A9})$$

$$\hat{a}_{A_0}^\dagger \rightarrow \frac{1}{\sqrt{2}} (\hat{a}_{A_0}^\dagger + \hat{a}_{A_1}^\dagger) \quad (\text{A10})$$

$$\begin{aligned} |\psi_\phi\rangle &= \frac{1}{\sqrt{2}} (|01\rangle_{A_0 B_1} + e^{i\phi} |10\rangle_{A_0 B_0}) \\ &\rightarrow \frac{1}{2} (|0010\rangle_{A_0 A_1 B_0 B_1} + |0001\rangle_{A_0 A_1 B_0 B_1} + e^{i\phi} |1000\rangle_{A_0 A_1 B_0 B_1} + e^{i\phi} |0100\rangle_{A_0 A_1 B_0 B_1}) \end{aligned} \quad (\text{A11})$$

Since this state has support on the single-photon Fock basis, we will define

$$\begin{aligned} |1000\rangle_{A_0A_1B_0B_1} &\equiv \begin{pmatrix} 1 \\ 0 \\ 0 \\ 0 \end{pmatrix}, & |0100\rangle_{A_0A_1B_0B_1} &\equiv \begin{pmatrix} 0 \\ 1 \\ 0 \\ 0 \end{pmatrix} \\ |0010\rangle_{A_0A_1B_0B_1} &\equiv \begin{pmatrix} 0 \\ 0 \\ 1 \\ 0 \end{pmatrix}, & |0001\rangle_{A_0A_1B_0B_1} &\equiv \begin{pmatrix} 0 \\ 0 \\ 0 \\ 1 \end{pmatrix} \end{aligned} \quad (\text{A12})$$

The density matrix can be written as

$$|\psi_\phi\rangle\langle\psi_\phi| = \frac{1}{4} \begin{pmatrix} 1 & 1 & e^{i\phi} & e^{i\phi} \\ 1 & 1 & e^{i\phi} & e^{i\phi} \\ e^{-i\phi} & e^{-i\phi} & 1 & 1 \\ e^{-i\phi} & e^{-i\phi} & 1 & 1 \end{pmatrix} \quad (\text{A13})$$

Let us examine effect of the channel on the the off-diagonal components, e.g

$$\begin{aligned} \mathcal{E}(|0010\rangle\langle 0001|) &= \int d\theta d\theta' \mu_{B_1}(\theta) \mu_{B_2}(\theta') e^{i\theta} e^{-i\theta'} |0010\rangle\langle 0001| \\ &= |\kappa|^2 |0010\rangle\langle 0001| \end{aligned} \quad (\text{A14})$$

Every off-diagonal component will pick up the same factor $|\kappa|^2$, therefore the density matrix becomes

$$\rho'_\phi = \mathcal{E}^{\otimes 4}(|\psi_\phi\rangle\langle\psi_\phi|) = \frac{1}{4} \begin{pmatrix} 1 & |\kappa|^2 & e^{i\phi}|\kappa|^2 & e^{i\phi}|\kappa|^2 \\ |\kappa|^2 & 1 & e^{i\phi}|\kappa|^2 & e^{i\phi}|\kappa|^2 \\ e^{-i\phi}|\kappa|^2 & e^{-i\phi}|\kappa|^2 & 1 & |\kappa|^2 \\ e^{-i\phi}|\kappa|^2 & e^{-i\phi}|\kappa|^2 & |\kappa|^2 & 1 \end{pmatrix} \quad (\text{A15})$$

We can apply \mathcal{F}^{-1} , which is simply two sets of 50:50 BS for two modes

$$F_2^{-1} = \frac{1}{\sqrt{2}} \begin{pmatrix} 1 & 1 & 0 & 0 \\ 1 & -1 & 0 & 0 \\ 0 & 0 & 1 & 1 \\ 0 & 0 & 1 & -1 \end{pmatrix} \quad (\text{A16})$$

We can diagonalise ρ'_ϕ . The eigenvalues and vectors are

$$\rho''_\phi = F_2^{-1} \rho'_\phi F_2^{-1\dagger} = \begin{pmatrix} \frac{1}{4}(1+|\kappa|^2) & 0 & \frac{1}{2}|\kappa|^2 e^{i\phi} & 0 \\ 0 & \frac{1}{4}(1-|\kappa|^2) & 0 & 0 \\ \frac{1}{2}|\kappa|^2 e^{-i\phi} & 0 & \frac{1}{4}(1+|\kappa|^2) & 0 \\ 0 & 0 & 0 & \frac{1}{4}(1-|\kappa|^2) \end{pmatrix} \quad (\text{A17})$$

We can see that the modes $|0100\rangle$ and $|0001\rangle$ are uncoupled, and these have 0 eigenvalues if $\kappa = 1$. The eigenvalues and vectors of ρ''_ϕ are

$$\begin{aligned} \frac{1}{4}(1-|\kappa|^2), & \quad [0, 0, 0, 1]^T \\ \frac{1}{4}(1-|\kappa|^2), & \quad [0, 1, 0, 1]^T \\ \frac{1}{4}(1-|\kappa|^2), & \quad \frac{1}{\sqrt{2}} [1, 0, -e^{-i\phi}, 0]^T \\ \frac{1}{4}(1+3|\kappa|^2), & \quad \frac{1}{\sqrt{2}} [1, 0, e^{-i\phi}, 0]^T \end{aligned} \quad (\text{A18})$$

We can compute the QFI , giving

$$I_Q = \frac{2|\kappa|^4}{|\kappa|^2 + 1} \quad (\text{A19})$$

What's the optimal measurement? Let us measure in the basis of $[A_0 \pm B_0]/\sqrt{2}, A_1, B_1$, so the basis set is $[1, 0, 1, 0]^T/\sqrt{2}, [1, 0, -1, 0]^T/\sqrt{2}, [0, 1, 0, 0]^T, [0, 0, 0, 1]^T$. The outcomes have probabilities

$$\begin{aligned} p_+ &= \frac{1}{4} (2|\kappa|^2 \cos(\phi) + |\kappa|^2 + 1) \\ p_- &= \frac{1}{4} (-2|\kappa|^2 \cos(\phi) + |\kappa|^2 + 1) \\ p_{A_2} &= \frac{1}{4} (1 - |\kappa|^2) \\ p_{B_2} &= \frac{1}{4} (1 - |\kappa|^2) \end{aligned} \quad (\text{A20})$$

The Fisher information is

$$\begin{aligned} \text{FI} &= -\frac{2|\kappa|^4 (|\kappa|^2 + 1) \sin^2(\phi)}{2|\kappa|^4 \cos(2\phi) + |\kappa|^4 - 2|\kappa|^2 - 1} \\ &= \frac{2|\kappa|^4}{|\kappa|^2 + 1} \quad \text{when } \theta \rightarrow \pi/2 \end{aligned} \quad (\text{A21})$$

Repeating for for $N = 3$, the QFI is

$$I_Q^{N=3} = \frac{3|\kappa|^4}{1 + 2|\kappa|^2} \quad (\text{A22})$$

3. N modes

If we use N modes, the encoded density matrix will take the form

$$\rho'_\phi = \begin{pmatrix} C & D \\ D^* & C \end{pmatrix} \quad (\text{A23})$$

where

$$C \equiv \frac{1}{2N} \begin{pmatrix} 1 & |\kappa|^2 & |\kappa|^2 \\ |\kappa|^2 & \dots & \dots \\ |\kappa|^2 & \dots & 1 \end{pmatrix}, \quad D \equiv \frac{e^{i\phi} |\kappa|^2}{2N} \begin{pmatrix} 1 & \dots & 1 \\ \dots & \dots & \dots \\ 1 & \dots & 1 \end{pmatrix}, \quad D^* \equiv \frac{e^{-i\phi} |\kappa|^2}{2N} \begin{pmatrix} 1 & \dots & 1 \\ \dots & \dots & \dots \\ 1 & \dots & 1 \end{pmatrix} \quad (\text{A24})$$

After the inverse QFT

$$\mathcal{F}^{-1}(N) = \begin{pmatrix} \mathcal{Q}^{-1}(N) & 0 \\ 0 & \mathcal{Q}^{-1}(N) \end{pmatrix} \quad (\text{A25})$$

$$\begin{aligned} \rho''_\phi &= \mathcal{F}^{-1} \rho'_\phi \mathcal{F} \\ &= \begin{pmatrix} \mathcal{Q}^{-1} & 0 \\ 0 & \mathcal{Q}^{-1} \end{pmatrix} \begin{pmatrix} C & D \\ D^* & C \end{pmatrix} \begin{pmatrix} \mathcal{Q} & 0 \\ 0 & \mathcal{Q} \end{pmatrix} \\ &= \begin{pmatrix} \mathcal{Q}^{-1} C \mathcal{Q} & \mathcal{Q}^{-1} D \mathcal{Q} \\ \mathcal{Q}^{-1} D^* \mathcal{Q} & \mathcal{Q}^{-1} C \mathcal{Q} \end{pmatrix} \end{aligned} \quad (\text{A26})$$

Since D and D^* are uniform, performing an inverse QFT gives a single component

$$\mathcal{Q}^{-1}D\mathcal{Q} = \frac{e^{i\phi}|\kappa|^2}{2} \begin{pmatrix} 1 & 0 & 0 \\ 0 & 0 & 0 \\ 0 & 0 & \dots \end{pmatrix}, \quad \mathcal{Q}^{-1}D^*\mathcal{Q} = \frac{e^{-i\phi}|\kappa|^2}{2} \begin{pmatrix} 1 & 0 & 0 \\ 0 & 0 & 0 \\ 0 & 0 & \dots \end{pmatrix} \quad (\text{A27})$$

Since only the coherent term between C and D contain information on ϕ , we only need to calculate $[\mathcal{Q}^{-1}C\mathcal{Q}]_{1,1}$. These matrices are highly symmetric, which simplifies the calculation:

$$\begin{aligned} \mathcal{Q}^{-1}C\mathcal{Q} &= \frac{1}{\sqrt{N}} \begin{pmatrix} 1 & 1 & 1 & 1 \\ 1 & e^{-i2\pi/N} & \dots & \dots \\ 1 & \dots & \dots & \dots \\ 1 & \dots & \dots & \dots \end{pmatrix} \times \frac{1}{2N} \begin{pmatrix} 1 & |\kappa|^2 & |\kappa|^2 & \dots \\ |\kappa|^2 & 1 & |\kappa|^2 & \dots \\ |\kappa|^2 & |\kappa|^2 & 1 & \dots \\ \dots & \dots & \dots & \dots \end{pmatrix} \times \frac{1}{\sqrt{N}} \begin{pmatrix} 1 & 1 & 1 & 1 \\ 1 & e^{i2\pi/N} & \dots & \dots \\ 1 & \dots & \dots & \dots \\ 1 & \dots & \dots & \dots \end{pmatrix} \\ \mathcal{Q}^{-1}C\mathcal{Q} &= \frac{1}{N} \begin{pmatrix} 1 & 1 & 1 \\ 1 & e^{-i2\pi/N} & \dots \\ 1 & \dots & \dots \end{pmatrix} \frac{1}{2N} \begin{pmatrix} 1 + (N-1)|\kappa|^2 & \dots & \dots \\ 1 + (N-1)|\kappa|^2 & \dots & \dots \\ 1 + (N-1)|\kappa|^2 & \dots & \dots \end{pmatrix} \end{aligned} \quad (\text{A28})$$

Therefore,

$$\mathcal{Q}^{-1}C\mathcal{Q}_{1,1} = \frac{1}{2N}(1 + (N-1)|\kappa|^2) \quad (\text{A29})$$

This means that we can examine only a 2 sub matrix of the density matrix to calculate the QFI:

$$\begin{pmatrix} [\mathcal{Q}^{-1}C\mathcal{Q}]_{1,1} & [\mathcal{Q}^{-1}D\mathcal{Q}]_{1,1} \\ [\mathcal{Q}^{-1}D\mathcal{Q}]_{1,1} & [\mathcal{Q}^{-1}C\mathcal{Q}]_{1,1} \end{pmatrix}. \quad (\text{A30})$$

The two eigenvalues and vectors that are sensitive to ϕ are

$$\begin{aligned} e_1 &= \frac{1 - |\kappa|^2}{2N}, \quad v_1 = [1, -e^{-i\phi}]^T / \sqrt{2} \\ e_2 &= \frac{1 + |\kappa|^2(2N-1)}{2N}, \quad v_2 = [1, e^{-i\phi}]^T / \sqrt{2} \end{aligned} \quad (\text{A31})$$

And the QFI is

$$\begin{aligned} I_Q^{(N)} &= \frac{N|\kappa|^4}{1 + |\kappa|^2(N-1)} \\ \lim_{N \rightarrow \infty} [I_Q^{(N)}] &= |\kappa|^2 \end{aligned} \quad (\text{A32})$$

We see that in the limit of large N , the QFI is boosted by a quadratic factor in $|\kappa|$ compared to the unencoded case.